

Received April 18, 2020; reviewed; accepted June 22, 2020

## Effect of particle size on chalcocite dissolution kinetics in column leaching under controlled Eh and its implications

Htet Aung Phy<sup>1,2,3,4</sup>, Yan Jia<sup>1,2,5</sup>, Qiaoyi Tan<sup>1,2,5</sup>, Shenggui Zhao<sup>4</sup>, Xinxing Liang<sup>4</sup>, Renman Ruan<sup>1,2,5</sup>, Xiaopeng Niu<sup>1,2</sup>

<sup>1</sup> CAS Key Laboratory of Green Process and Engineering, Institute of Process Engineering, Chinese Academy of Sciences, Beijing 100190, PR China

<sup>2</sup> National Engineering Laboratory for Hydrometallurgical Cleaner Production Technology, Chinese Academy of Sciences, Beijing 100190, PR China

<sup>3</sup> University of Chinese Academy of Sciences, Beijing 10049, PR China

<sup>4</sup> Wanbao Mining Ltd, Beijing 100053, PR China

<sup>5</sup> State Key Laboratory of Biochemical Engineering Institute of Process Engineering, Chinese Academy of Sciences, Beijing 100190, PR China

Corresponding author: xpniu@ipe.ac.cn (Xiaopeng Niu)

**Abstract:** Natural high grade chalcocite samples were leached in column under controlled Eh, constant temperature and solution pH to investigate the effect of particle size on dissolution kinetics. Moreover, low grade ores of larger size fractions were leached in column using raffinate from the industrial heap as an irrigation solution to simulate the real heap conditions. The leaching rate of large particle sizes (31-200 mm) were very slow without inflection point which are normally present in the leaching of small particle sizes (0.054-31 mm). The effect of particle size was more remarkable in the dissolution of large particles than that of small particles during the first stage (<45% dissolution). However, the dissolution rate of the second stages (>45% dissolution) were not noticeably affected by the particle size. Results of kinetics analysis of leaching of small particles using shrinking core model indicated that the first stage was controlled by fluid diffusion and confirmed by the low activation energies (20.98 kJ/mol). The kinetics of second stage was controlled by chemical reaction and product layer diffusion and the later control became prominent with increasing particle size. Similarly, product layer diffusion was the rate-controlling step for the first and second stages of leaching of large particles. X-ray CT and SEM-EDS studies observed the increasing numbers of cracks and porosity and the formation of sulfur layer on the surface of the residue samples. The findings in this study provided some useful implications to optimize the heap performance and understand the leaching behavior of large particles.

**Keywords:** particle size, column leaching, chalcocite, shrinking core model, X-ray CT

### 1. Introduction

Chalcocite ( $\text{Cu}_2\text{S}$ ) is the most common secondary copper sulfide that contains the highest copper content and can be extracted with heap bioleaching which is simple, less energy-intensive and efficient for the processing of low grade ore and large particle sizes compared to other extraction techniques (Brierley, 2001; Ghorbani et al., 2011; Toro et al., 2019). Although this method has been widely used in industry, there are some limitations such as slow leaching kinetics, low recoveries, longer extraction time and high operation cost due to acid consumption (Ogbonna et al., 2006; Watling, 2006; Petersen, et al., 2007). In order to mitigate these problems, it is essential to understand the kinetics of leaching in the heap (Crundwell, 2013). Hence, the leaching kinetics of chalcocite in acidic ferric sulfate media has been extensively studied and reported that chalcocite dissolution occurred in two distinct stages (Eqs. 1, 2) (Bolorunduro, 1999; Miki et al., 2011; Castillo et al., 2019).



The first stage is the conversion of chalcocite into blue-remaining covellite (CuS) via the formation of a series of intermediate products and is very rapid and controlled by diffusion of ferric ion through liquid film around the particle that was supported by low activation energies (4-25 kJ/mol) (Cheng et al., 1991b; Naderi et al., 2015; Pérez et al., 2020). In the second stage, covellite is oxidized to produce cupric ion and more than 90% of the sulfide moiety are transformed to elemental sulphur and the rate is very slow and sensitive to temperature (Schippers et al., 1999; Miki et al., 2011; Fang et al., 2018). The rate-controlling step for the second stage is not fully understood and some previous studies on chalcocite dissolution kinetics adopted the stirred leaching whereas the column leaching can help to simulate the operating parameters for heap leaching. In addition, the redox potential of solution (Eh) significantly dropped at the beginning of the reaction due to the rapid consumption of oxidant and most studies failed to control the solution Eh while iron-oxidizing bacteria in the real heap maintain the solution Eh at a steady level. Hence, the authors investigated chalcocite dissolution in column leaching under controlled Eh and reported that temperature is more sensitive to dissolution rather than Eh and ferric concentration (Niu et al., 2015). Moreover, the dissolution was found to have two inflection points at 45 and 70% dissolution which indicated the shift of rate-controlling step during the leaching process of fine particles (0.03-0.074 mm). The effect of particle size on dissolution kinetics was not fully understood although the inflection behavior of dissolution seemed to be dependent of particle size (Cheng et al., 1991a; Bolorunduro, 1999; Aracena et al., 2019).

It is generally believed that ore particle size affects the leaching kinetics and the change in particle size has inversed square effect on the leaching rate and recovery increases with decreasing particle size (Suni et al., 1989; Bolorunduro, 1999; Miller, 2003). Some studies reported that the particle size only influenced the first stage and its effect significantly decreases during second stage due to interfacial reaction areas (Bolorunduro, 1999; Hashemzadeh et al., 2019). On the other hand, some argued that the leaching rate is independent of particle size (Strömberg et al., 1999; Mazuelos et al., 2001; Deveci et al., 2004). In summary, most of previous studies had only reported dissolution kinetics for relatively small particle sizes ranging from 0.011 to 0.5 mm although the top size of the industrial heaps are 50-180 mm for crushed ores and 1-2 m for run-of-mine ores. Therefore, these studies were not able to elucidate the leaching behavior of large ore. In addition, there is no literature which reports dissolution kinetics of large particles and mineralogical changes during leaching despite the fact that leaching of large particles are assumed to follow shrinking core behavior and occur only at the mineral surface and in subsurface regions through accessible cracks and pores from the surface (Liddell et al., 2005; Malmström et al., 2008; Ghorbani et al., 2011).

This study was attempted to investigate the effects of particle size on dissolution kinetics in column leaching under controlled Eh and to determine the rate-controlling steps for the kinetics of chalcocite leaching. Therefore, column leaching experiments of high grade chalcocite ore were conducted under controlled Eh, high ferric concentration, constant pH and temperature reported by the previous study at optimum conditions for chalcocite dissolution (Niu et al., 2015). Furthermore, low grade chalcocite ores were also leached in columns using raffinate from an industrial heap to simulate the real heap conditions. The results would deepen the understanding of the leaching behaviors of large particles that helps to optimize the performance of commercial heap.

## 2. Materials and methods

### 2.1. Minerals

High grade chalcocite mineral from Myanmar Wanbao Mining was used to conduct the chemical leaching in column. Firstly, the sample was crushed and ground, then screened into six size fractions (-0.074+0.054, -0.105+0.074, -0.5+0.105, -1+0.5, -2+1, -4+2 mm). XRD analysis confirmed that the main mineral phase was chalcocite (Fig. 1) and the chemical analysis of each size fraction is given in Table 1. The stability of copper grade at all particle sizes is indicative of the complete liberation of chalcocite mineral. The crushed samples were kept in nitrogen environment to avoid surface oxidation.

For column bioleaching experiments, the low-grade ore from Monywa copper mine in Myanmar was used. The ore was crushed and screened into six different size fractions (-9.5+3.35, -19+9.5, -31+19, -50+19, -90+50 and -200+50 mm). Table 2 summarized the chemical composition of different size of ore samples. The copper grade of different particle size was not uniform due to the nature of low grade ore and the large size.

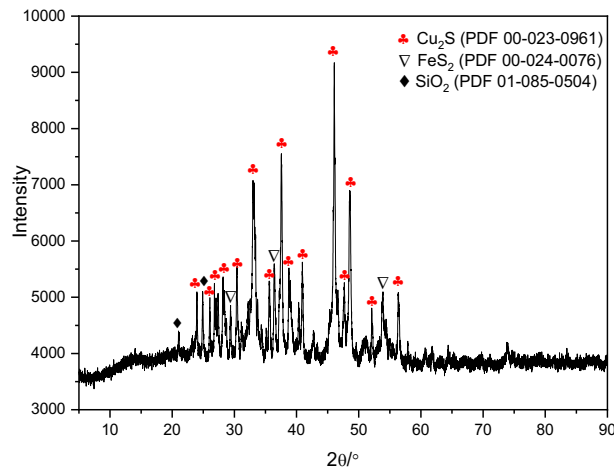


Fig. 1. X-ray pattern of chalcocite mineral (- 0.105+0.074 mm)

Table 1. Chemical analysis of different-sized fractions of high grade chalcocite samples (wt.%)

Size Fraction (mm)	Cu	S	Fe	SiO <sub>2</sub>
- 0.074 +0.054	64.94	21.75	5.42	3.99
-0.105 +0.074	60.31	26	10.56	0.94
-0.5 +0.105	60.46	26.1	9.83	1.05
-1 +0.5	60.11	24.22	10.52	1.4
-2 +1	59.13	25.44	11.14	1.18
-4 +2	59.6	25.24	10.98	1.34

Table 2. The chemical composition of different size fractions of low-grade ore (wt.%)

Size Fraction (mm)	Cu	Fe
- 9.5+3.5	1.67	7.66
-19+9.5	0.54	5.92
-31+19	0.66	5.12
-50+31	0.42	6.2
-90+50	0.57	5.36
-200 +90	0.94	6.29

## 2.2. Column leaching experiment

Chemical leaching experiments were carried out in glass columns shown in Fig. 2 and the experimental procedure were adapted from the previous study (Niu et al., 2015). 2 g of high grade chalcocite sample was leached under controlled Eh of 750 mV (Vs SHE), pH 1±0.5 and temperature of 45 °C. To avoid the depletion of ferric ion during reaction, 10 g/dm<sup>3</sup> of ferric ion was used as the main oxidizing agent. As recent studies suggested that the concentration of sulfuric acid only had minimal effect on copper dissolution (Cheng et al., 1991b; Pérez et al., 2020), 10 g/dm<sup>3</sup> of 98 wt% H<sub>2</sub>SO<sub>4</sub> was used to simulate the acidity of industrial heap. The controlled Eh was adjusted within 750 ± 5 mV of set value by adding 7.5 wt% H<sub>2</sub>O<sub>2</sub> and pH was adjusted using H<sub>2</sub>SO<sub>4</sub>. For the temperature control, the reactor flask was heated by oil bath equipped with thermostat and glass column was regulated by using water bath. During leaching experiments, solution samples (2 cm<sup>3</sup>) were removed periodically. After finishing the leaching experiments, the leached residues were washed with pH 1 solution and kept under nitrogen atmosphere

for subsequent analysis. The analytical grade  $\text{Fe}_2(\text{SO}_4)_3$ ,  $\text{H}_2\text{SO}_4$  and  $\text{H}_2\text{O}_2$  were used for the preparation of leaching solution and controlling pH and Eh.

For column bioleaching experiments, 40 kg of low grade ores were leached in steel column at ambient temperature ( $35\text{ }^\circ\text{C}$ ) by continuously irrigating raffinate from solvent extraction plant of Monywa mine at a rate of  $3.67\text{ cm}^3/\text{min}$ . The previous study reported that the dominant microbial community in raffinate solution was *Ferroplasma* and other microbial species (Jia et al., 2018). The same microbial groups were fed daily and their activity was checked with optical microscope. The raffinate and leachate were sampled daily to measure the concentration of copper, ferrous and ferric. The average results of physiochemical parameters of irrigation solution are shown in Table 3. These experiments were open cycle using the same daily raffinate to maintain Eh and followed the procedure presented in previous study (Jia et al., 2018).

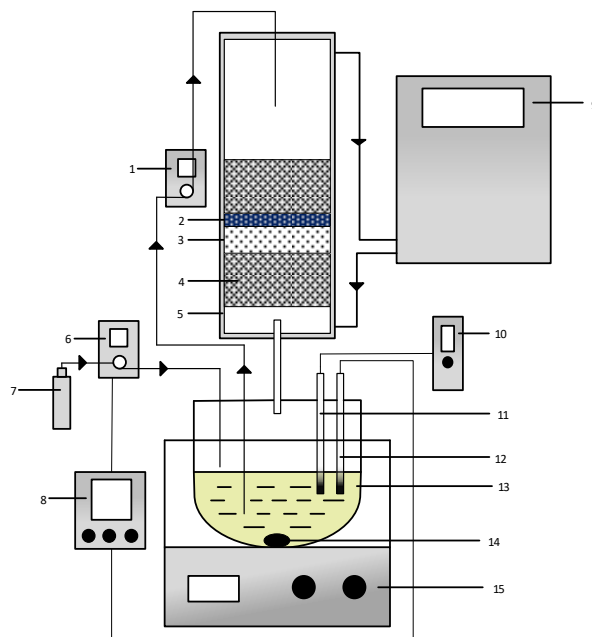


Fig. 2. A schematic of column leaching setup under controlled Eh and pH, 1-pump, 2-chalcocite, 3-silica, 4-glass beads, 5-water-jacket, 6- pump, 7-  $\text{H}_2\text{O}_2$ , 8-Eh controller, 9-water bath, 10-pH meter, 11-pH electrode, 12-Eh electrode, 13-five-necked flask, 14-magnet, 15-oil bath with stirrer

Table 3. Physiochemical assays of the irrigation solution

Parameter	Average
Cu ( $\text{g}/\text{dm}^3$ )	0.72
Free acid ( $\text{g}/\text{dm}^3$ )	9.93
Total iron ( $\text{g}/\text{dm}^3$ )	13.96
$\text{Fe}^{3+}$ ( $\text{g}/\text{dm}^3$ )	13.93
$\text{Fe}^{2+}$ ( $\text{g}/\text{dm}^3$ )	0.03
pH	1.54
Eh (mV)	664

### 2.3. Kinetics modelling

The dissolution kinetics of chalcocite was studied to understand the rate-controlling step and to optimise the leaching process. As chalcocite leaching is heterogeneous reaction including more than one phase, specifically fluid and solid phase, shrinking core model (SCM) (Levenspiel, 1999) for spherical particles of unchanging size can be used to study the kinetics. The particle should be spherical and remain constant in shape during reaction to satisfy the requirements for SCM. The concentration of solid reactant in unreacted core is also assumed to be constant (Nazemi et al., 2011). According to SCM, there are three steps controlling the reaction which include no gaseous products. These steps are:

Step 1: Diffusion of leaching oxidant through the liquid film surrounding particle.

$$x = k_f t \quad (3)$$

Step 2: Diffusion of leaching oxidant through the product layer at the surface of unreacted core.

$$1 - 3(1 - x)^{\frac{2}{3}} + 2(1 - x) = k_p t \quad (4)$$

Step 3: Chemical reaction of the oxidant with unreacted core at the surface.

$$1 - (1 - x)^{\frac{1}{3}} = k_c t \quad (5)$$

where  $x$  is the fractions of reacted solid particles,  $k_f$ ,  $k_p$  and  $k_c$  are apparent rate constants for the different rate controlling steps and  $k_f = \frac{3bk_l C_{fs}}{\rho r_0}$ ,  $k_p = \frac{6MbD_e C_{fs}}{\rho r_0^2}$ ,  $k_c = \frac{Mb k_c C_{fs}}{\rho r_0}$ , and  $t$  is the reaction time.

If one step has highest resistance to reaction, this step is considered as rate-controlling step. Levenspiel (1999) stated equations (Eqs. 3-5) to determine the reaction rate for the above three steps. From the plot of the left hand side of each equation against time using experimental data, the equation with the correlation coefficient ( $R^2$ ) of closest to 1 is considered to be the rate-controlling step for the system. The shrinking core model and its rate-controlling equations were used to analyze the dissolution data of different particle sizes ranging from 0.054 to 200  $\mu\text{m}$  by linear regression using least square method. The determination of rate-controlling step can be verified by the value of activation energies and, therefore, the activation energies were calculated by the Arrhenius equation.

$$k = A e^{\left(\frac{-E_a}{RT}\right)} \quad (6)$$

where  $k$  is the rate constant,  $A$  is the frequency factor,  $E_a$  is the activation energy (kJ/mol),  $R$  is the universal gas constant (J/mol.K), and  $T$  is the absolute temperature (K).

## 2.4. Characterization

Inductively coupled plasma optical emission spectrometry (ICP-OES) was used to measure total copper (Cu) and iron (Fe) concentration. The ferrous concentration was titrated with potassium dichromate and the ferric concentration was calculated from the difference between total Fe and ferrous concentration. The solution Eh and pH were checked using a FermProbe Pt electrode with Ag/AgCl reference electrode (3.8 M KCl) and Mettler Toledo SG8 pH electrode. The structural changes of mineral sample before and after leaching were examined using X-ray computed tomography (X-ray CT) because it can give the 3-D mineral dissemination and crack distribution in the solid objects (Geet et al., 2000; Videla et al., 2007). Xradia 410 Versa X-ray CT scanner was used at 120 keV of X-ray source with pixel size of 3.67  $\mu\text{m}$  and exposure time of 5 seconds at 0.0075° rotation. The magnification used was 4X. The results of mineralogical changes and surface studies by X-ray CT are evaluated using scanning electron microscopy (SEM)-energy dispersive spectroscopy (EDS) and X-ray diffraction (XRD). Rigaku Smartlab X-ray diffractometer was operated at 45 kV and 200 mA for collection of the phases of residues from 5° to 90° (2 $\theta$ ) with a scan rate of 0.2 °/s. Original and residue samples were coated with platinum by electrodeposition and the microstructures were studied by SEM (JSM-7001, Japan) coupled with EDS (INCAX-MAX) at 15 kV accelerating voltage.

## 3. Results and discussion

### 3.1. Effect of particle size in chemical leaching

The different particle size fractions (0.054-4 mm) as shown in Table 1 of high grade chalcocite were leached in glass columns to study the effect of particle size on chalcocite dissolution kinetics under controlled redox potential and moderate temperature of 45 °C. Fig. 3a and 3b illustrate the effect of particle size on first stage and second stage of chalcocite dissolution. It can be seen from Fig. 3a that particle size had significant effect on the dissolution and the duration to finish the first stage was quite fast. For instance, the dissolution of -0.074+0.054 mm only needed about 2.5 hours while the approximate duration of 17 hours was required for -4+2 mm. Hence, it can be concluded that the larger particle needs more time to achieve the corresponding dissolution than smaller particles. From the second stage of chalcocite dissolution shown in Fig. 3b, it was evident that dissolution kinetics increases with decreasing particle size and this finding were consistent with the postulation. Therefore, the final

Cu dissolution values were 85% for -4+2 mm and 95% for -0.074+0.054 mm during same leaching time. Another interesting finding was that the dissolution curves of second stage had the inflection point around 75% Cu dissolution and the dissolution lower and higher than this point were distinct. The inflection points were not the same for different particle sizes and the similar behavior was also reported in previous studies (Cheng et al., 1991a; Niu et al., 2015). Hence, the dissolution between 45 and 75% was noted as the first sub-stage and dissolution beyond 75% as second sub-stage. The dissolution rate of first sub-stage was found to be about 20 times faster compared to that of second sub-stage and this behaviors were the same for all particle size fractions. Therefore, it can be concluded that initial particle size influenced the first stage to a large degree and on the first sub-stage to a slight degree. However, particle size effect on second sub-stage was no noticeable.

To investigate the effect of particle size on the dissolution rate, the dissolution data in Fig. 3a and 3b were used to calculate the dissolution rate and the results were presented in Fig. 4a using linear regression. The first noticeable thing was the negative slope indicating the decline of dissolution rate for larger particles. By comparing the value of slope of each stage, it can be noted that the dissolution rate of first stage had half order dependence on the particle size while the dependence of rate of first sub-stage and second sub-stage were not obviously found. Besides, the effect of particle size on the second sub-stage was found to be the smallest among three stages and hence it suggested that the particle size was not related to dissolution mechanisms during second sub-stage and similar findings was reported for the leaching of size fractions (0.053-0.212 mm) (Hashemzadeh et al., 2019). Fig 4b presents the calculated activation energies for each stage in chalcocite dissolution, which showed the first stage only needed least amount of energies rather than other second stages. Since activation energies depend on the reaction temperature (Eq. 6), it could be noted that the first stage is not sensitive to temperature unlike first sub-stage and second sub-stage.

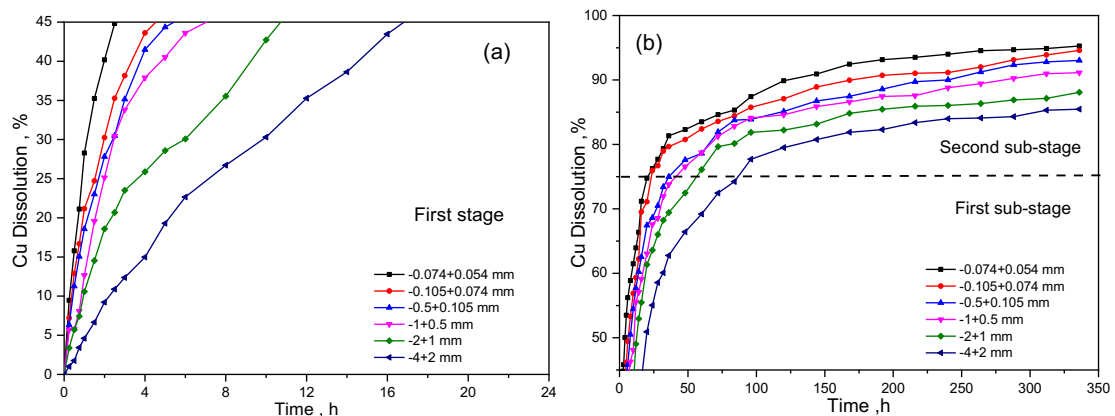


Fig. 3. Cu dissolution of different particle size of high grade chalcocite ore in two distinct stages: (a) first stage, (b) second stage ( $[\text{Fe}^{3+}] = 10 \text{ g/dm}^3$ ,  $\text{pH} = 1.00\sim 1.50$ ,  $E_h = 750 \text{ mV}$ , temperature =  $45^\circ \text{C}$ )

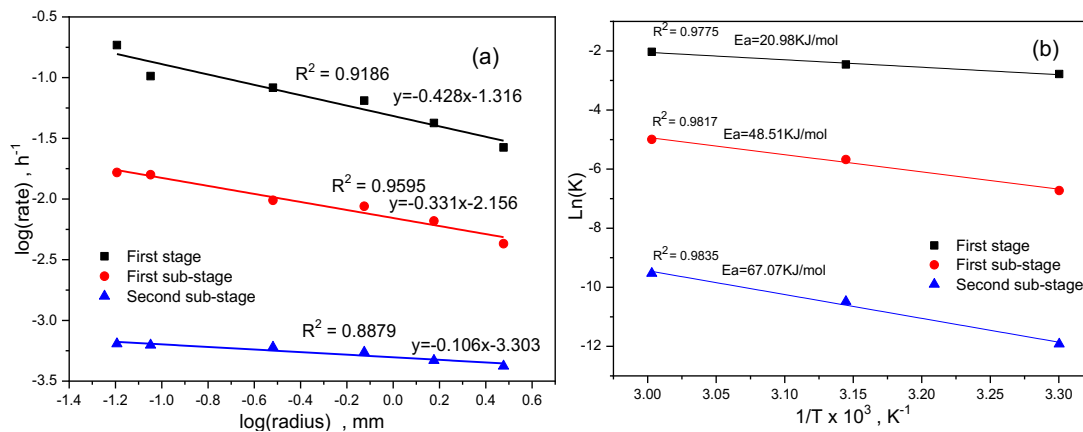


Fig. 4. a) Effect of particle size on the dissolution rate of chalcocite of each stage, b) Arrhenius plot for the chalcocite dissolution

Fig. 5 shows the kinetic plot for dissolution of first stage and it can be seen that the copper dissolution was a linear function of time and this linear relationship suggested that the first stage was controlled by film diffusion. This was confirmed by low activation energies of 20.98 kJ/mol from an Arrhenius plot shown in Fig. 4b and agrees with previous studies (Cheng et al., 1991a; Crundwell et al., 2013; Hashemzadeh et al., 2019). The specific rate constants were calculated from the slope of the curves and the known values of other quantities. The apparent and specific rate constants and correlation coefficient of dissolution of each particle size were shown in Table 4. It could be noted that the specific rate constants decrease for smaller particle sizes and indicated that the film diffusion control was more prominent in the dissolution of small particle sizes (Cheng et al., 1991a).

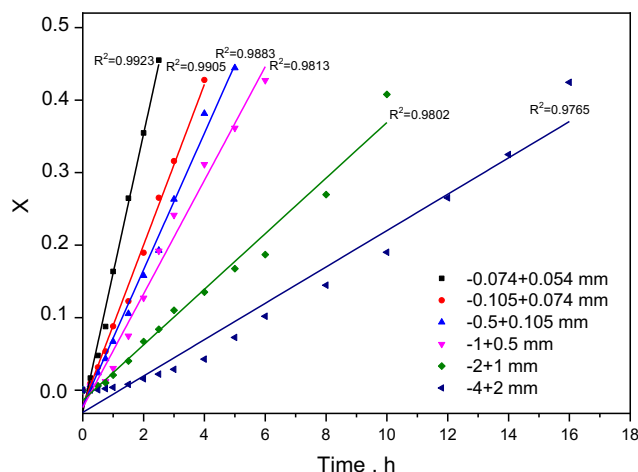


Fig. 5. Kinetic plot of film diffusion for first stage dissolution ( $[\text{Fe}^{3+}] = 10 \text{ g/dm}^3$ ,  $\text{pH} = 1.00\sim 1.50$ ,  $\text{Eh} = 750 \text{ mV}$ , temperature =  $45 \text{ }^\circ\text{C}$ )

Table 4. The apparent rate constant and coefficient of kinetics of first stage ( $[\text{Fe}^{3+}] = 10 \text{ g/dm}^3$ ,  $\text{pH} = 1.00\sim 1.50$ ,  $\text{Eh} = 750 \text{ mV}$ , temperature =  $45 \text{ }^\circ\text{C}$ )

Particles size (mm)	Film diffusion control, X		
	R <sup>2</sup>	K <sub>f</sub> (1/min)	K <sub>L</sub> (1/cm <sup>2</sup> min)
- 0.074 +0.054	0.9923	$2.89 \times 10^{-3}$	$1.94 \times 10^{-4}$
-0.105 +0.074	0.9905	$1.74 \times 10^{-3}$	$1.64 \times 10^{-4}$
-0.5 +0.105	0.9883	$1.43 \times 10^{-3}$	$4.54 \times 10^{-4}$
-1 +0.5	0.9813	$1.25 \times 10^{-3}$	$9.89 \times 10^{-4}$
-2 +1	0.9802	$6.65 \times 10^{-4}$	$1.05 \times 10^{-3}$
-4+2	0.9765	$4.52 \times 10^{-4}$	$1.43 \times 10^{-3}$

The kinetics of second stage was very different from that of the first stage and the Cu dissolution became nearly stable around 75% of dissolution. The kinetics of first sub-stage for different particle sizes were demonstrated in Fig. 6a-b. Fig. 6a provided convincing evidence showing that R<sup>2</sup> for chemical reaction control for leaching of smaller particles was closer to 1 than that of larger particles. Accordingly, it was concluded that the dissolution process was controlled by chemical reaction at the beginning of the first sub-stage but chemical reaction control diminished as the particle size increases. For larger particles, Fig. 6b describes that R<sup>2</sup> for diffusion through product layer became closer to 1 which showed the diffusion control was more prominent. Therefore, it could be noted that the reaction control mechanisms shift from chemical reaction to product layer diffusion for larger particles. The reason for that postulation is that the length of the diffusion of oxidant from the liquid film around the particle to the surface of the unreacted core of large particle size was lengthened compared to small particle size. The calculated apparent rate constants were tabulated in Table 5 and it could be noted that the specific constant for chemical reaction was found to be independent of particle size and the rate constant for diffusion control process was sensitive to the changes in particle size. These calculated values support the postulation of shrinking core model (Bobbeck et al., 1985).

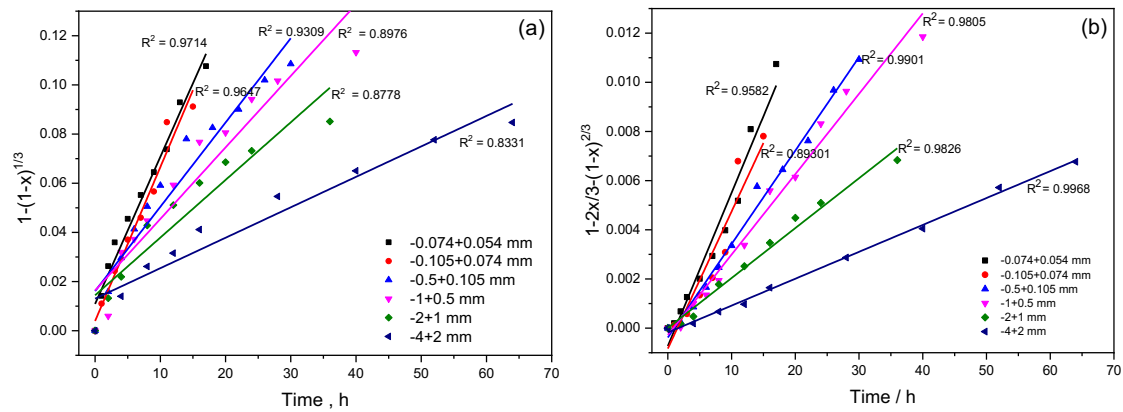


Fig. 6. Plot of (a):  $1-(1-x)^{1/3}$  and (b):  $1-2x/3-(1-x)^{2/3}$  for first sub-stage of Cu dissolution for different particle size ( $[\text{Fe}^{3+}] = 10 \text{ g/dm}^3$ ,  $\text{pH} = 1.00\text{--}1.50$ ,  $E_h = 750 \text{ mV}$ , temperature =  $45^\circ\text{C}$ )

Table 5. The apparent rate constant and coefficient of kinetics of first sub-stage ( $[\text{Fe}^{3+}] = 10 \text{ g/dm}^3$ ,  $\text{pH} = 1.00\text{--}1.50$ ,  $E_h = 750 \text{ mV}$ , temperature =  $45^\circ\text{C}$ )

Particles size (mm)	Chemical reaction control, $1-(1-X)^{1/3}$			Product layer diffusion control, $1-3(1-X)^{2/3}+2(1-X)$		
	$R^2$	$K_c$ (1/min)	$K_{cc}$ (cm/min)	$R^2$	$K_p$ (1/min)	$D_e$ ( $\text{cm}^2/\text{min}$ )
- 0.074 +0.054	0.97139	$9.98 \times 10^{-5}$	$1.27 \times 10^{-7}$	0.95817	-	-
-0.105 +0.074	0.96465	$1.04 \times 10^{-4}$	$1.85 \times 10^{-7}$	0.89301	-	-
-0.5 +0.105	0.93087	-	-	0.9911	$6.34 \times 10^{-6}$	$5.75 \times 10^{-10}$
-1 +0.5	0.89762	-	-	0.98047	$5.45 \times 10^{-6}$	$3.04 \times 10^{-9}$
-2 +1	0.8778	-	-	0.98258	$3.38 \times 10^{-6}$	$7.54 \times 10^{-9}$
-4+2	0.83311	-	-	0.99682	$1.82 \times 10^{-6}$	$1.63 \times 10^{-8}$

It is clear from Fig. 7 that the second sub-stage was controlled by diffusion through elemental sulfur layer by evaluating the  $R^2$  for different particle sizes. A similar result was reported that the diffusion control becomes prominent during second sub-stage (Ruiz et al., 1998; Niu et al., 2015). From the Arrhenius plot shown in Fig. 4b, the apparent activation energy of  $67.07 \text{ kJ/mol}$  was obtained for second sub-stage. Table 6 shows the constant and effective diffusivity of each particle fraction in second sub-stage dissolution and their values decrease with decreasing particle size and indicated that the diffusion barrier i.e. the elemental sulfur layer, was supposed to be thicker for small particles.

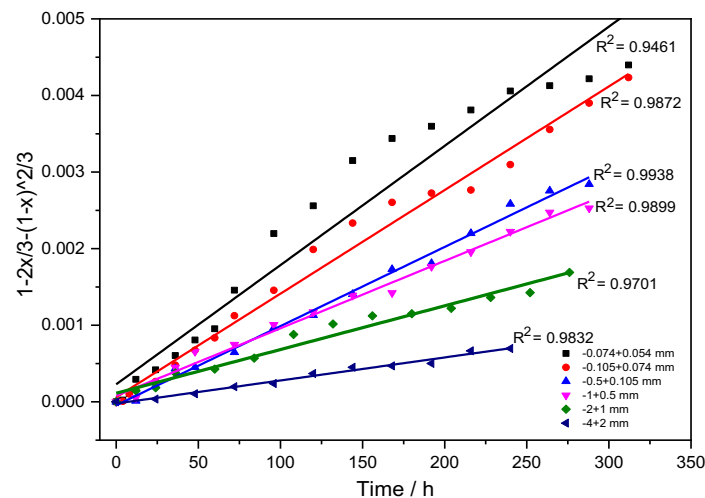


Fig. 7. Plots of  $1-2x/3-(1-x)^{2/3}$  versus time for the second sub-stage of Cu dissolution for different particle sizes ( $[\text{Fe}^{3+}] = 10 \text{ g/dm}^3$ ,  $\text{pH} = 1.00\text{--}1.50$ ,  $E_h = 750 \text{ mV}$ , temperature =  $45^\circ\text{C}$ )

Table 6. The apparent rate constant and coefficient of kinetics of second sub-stage ( $[\text{Fe}^{3+}] = 10 \text{ g/dm}^3$ ,  $\text{pH} = 1.00\text{--}1.50$ ,  $E_h = 750 \text{ mV}$ , temperature =  $45 \text{ }^\circ\text{C}$ )

Particles size (mm)	Product layer diffusion control, $1-3(1-X)^{2/3}+2(1-X)$		
	$R^2$	$K_p$ (1/min)	$D_e$ ( $\text{cm}^2/\text{min}$ )
- 0.074 +0.054	0.9923	$2.59 \times 10^{-7}$	$1.05 \times 10^{-12}$
-0.105 +0.074	0.9905	$2.25 \times 10^{-7}$	$1.79 \times 10^{-12}$
-0.5 +0.105	0.9883	$1.72 \times 10^{-7}$	$1.56 \times 10^{-11}$
-1 +0.5	0.9813	$1.47 \times 10^{-7}$	$8.18 \times 10^{-11}$
-2 +1	0.9802	$9.51 \times 10^{-8}$	$2.12 \times 10^{-10}$
-4+2	0.9765	$5.01 \times 10^{-8}$	$4.47 \times 10^{-10}$

### 3.2. Effect of particle size in column bioleaching

Column bioleaching experiments were conducted to study the effect of particle size on leaching kinetics and results are shown in Fig. 8a. The final dissolution of -200+90 mm size was only 61% while that of -9.5+3.5 mm size reached about 92%. Two inflections points only occurred in three smaller sizes (-9.5+3.5, -19+9.5 and -31+19 mm) and there is no inflection point for larger particle sizes (31-200 mm) even though the dissolution was achieved more than 45%. This may be due to the slow dissolution rate and lack of the shift of rate-controlling step in the leaching of large particles. Another finding in Fig. 8a was that the dissolution rate of -50+31 mm and -90+50 mm were similar and it may be because of the inconsistency of copper composition present in ore. The dissolution rate of the largest particle size (+90-200 mm) was six times slower than that of the smallest particle size (+3.5-9.5 mm) within the range of first stage. Among the dissolution of three smaller particle sizes, the dissolution of -31+19 mm needs three-fold time of that of -9.5+3.5 mm to finish its first sub-stage.

The dissolution rate of second stage was found slightly affected by particle size. This behavior was seen in Fig. 8b which shows the effect of particle size on dissolution rate of first stage in consistent with the result of chemical leaching of high grade ore under controlled redox potential. The slope of 0.619 for first stage indicated that dissolution of large particles were more sensitive to particle size than small particles (slope of 0.428). The effect of particle size for second stage was not obvious and this may be because of the breakage of the large particles into smaller ones and this was confirmed by the mineralogical studies which were discussed in section 3.4. The experimental data from Fig. 8a were also used to investigate the effect of particle size on the rate-controlling step during the leaching process. Table 7 shows the correlation coefficients ( $R^2$ ) of the fitted data for each stage of chalcocite dissolution using the equations of SCM (Eqs. 3-5). It was found that the  $R^2$  values were similar for each rate controlling steps during the fitting process for different size fractions. This may be due to the low copper content in the ore and the increasing particle size which cause the slowness of dissolution rate.

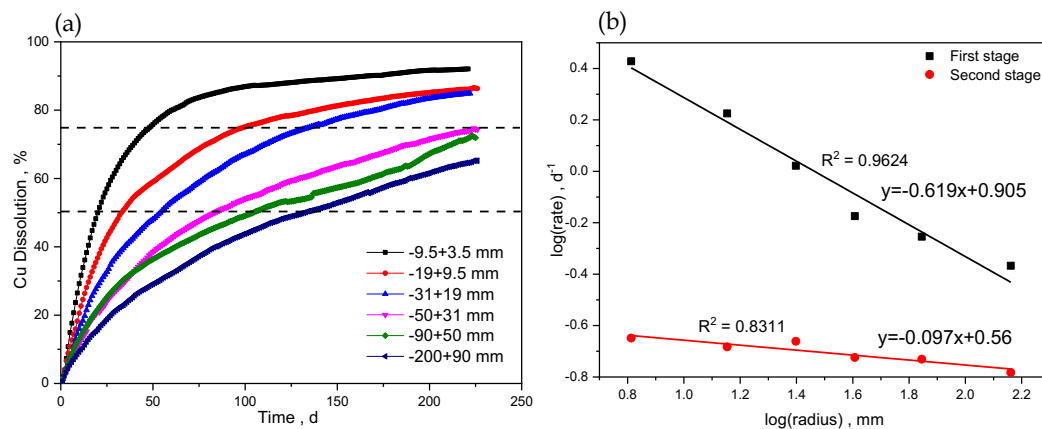


Fig. 8. a) Cu dissolution of different particle size low grade chalcocite ore ( $[\text{Fe}^{3+}] = 13.93 \text{ g/dm}^3$ ,  $\text{pH} = 1.54$ ,  $E_h = 664 \text{ mV}$ , temperature =  $35 \text{ }^\circ\text{C}$ ), b) Effect of particle size on dissolution rate during column bioleaching of low grade chalcocite ore

Table 7. Correlation coefficients values of shrinking core kinetic models for bioleaching of low grade chalcocite ore ( $[\text{Fe}^{3+}] = 13.93 \text{ g/dm}^3$ ,  $\text{pH} = 1.54$ ,  $\text{Eh} = 664 \text{ mV}$ , temperature =  $35 \text{ }^\circ\text{C}$ ).

Particle Size, mm	Correlation coefficient for evaluated models, $R^2$		
	X	$1-(1-X)^{1/3}$	$1-3(1-X)^{2/3}+2(1-X)$
First stage (0-45% Cu dissolution)			
-9.5+3.5	0.9897	0.9967	0.9300
-19+9.5	0.9847	0.9946	0.9581
-31+19	0.9628	0.9796	0.9831
-50+31	0.9701	0.9778	0.9856
-90+50	0.9266	0.9517	0.9980
-200+90	0.9658	0.9824	0.9835
First sub-stage (45-75% Cu dissolution)			
-9.5+3.5	0.9665	0.9771	0.9911
-19+9.5	0.9778	0.9859	0.9861
-31+19	0.9816	0.9890	0.9823
-50+31	0.9880	0.9754	0.9936
-90+50	0.9863	0.8785	0.9909
-200+90	0.9987	0.9430	0.9990
Second sub-stage (Above 75% Cu dissolution)			
-9.5+3.5	0.8443	0.8567	0.9692
-19+9.5	0.9753	0.9783	0.9893
-31+19	0.9862	0.9880	0.9769

rate. However, it still can be concluded that the first stage of dissolution of particle size between 3.5 and 31 mm was controlled by chemical reaction by evaluating the  $R^2$  values. Otherwise,  $R^2$  values for diffusion control were closer to one during the first sub-stage and it suggested that the chemical reaction control shifted to diffusion control since large particles undergone the breakage during the first sub-stage and consequently causing the increase of surface area which attributed to chemical reaction faster. Similarly, diffusion through product layer controlled the kinetics of the second sub-stage dissolution of particle sizes between 3.5 to 31 mm and this result agrees with the results obtained from the chemical leaching of high grade chalcocite ore. On the other hand, the dissolution of particle sizes larger than 31 mm were assumed to be controlled by one rate controlling step due to the lack of inflection point on the dissolution curves which indicated no alteration of kinetics in both first stage and second stage. In addition, the  $R^2$  values also suggested that product layer diffusion control was prominent during first and second stages since the gangue mineral present in the leached low grade ore act as elemental sulfur layer which were formed in the later stage of dissolution. Hence, it could be noted that the changes in reaction control mechanisms were obvious in the dissolution of small particles even though product layer diffusion control was the only rate-limiting stage during the dissolution of large particles. These findings suggested that the leaching of large particle size followed the shrinking core behavior and the product layer diffusion control becomes more significant.

### 3.3. Effect of temperature in chemical leaching

To determine the effect of temperature on chalcocite dissolution kinetics, -0.5+0.105 mm size fraction of chalcocite samples were leached at temperatures ranging from 30 to  $60^\circ\text{C}$  and the results were presented in Fig. 9. At high temperature ( $60^\circ\text{C}$ ), dissolution reached more than 94% in 72 hours while it took 336 hours at  $45^\circ\text{C}$ . The main observation here was that the dissolution rate for second stage at low temperature  $30^\circ\text{C}$  was about half of that at  $60^\circ\text{C}$  and showing that temperature had prominent effect on second stage leaching. The inflection point which distinguishes first sub-stage and second sub-stage has occurred at low dissolution level in leaching at  $30^\circ\text{C}$ . It was well noted that only one inflection point appeared in the dissolution at  $60^\circ\text{C}$  and this translated into a shorter time was needed to yield higher dissolution than at low temperature.

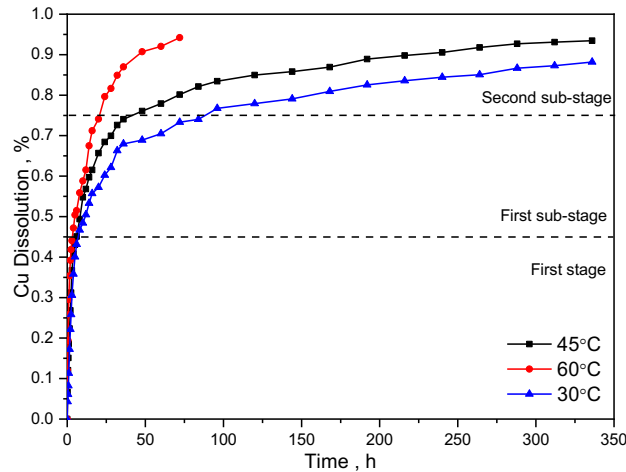


Fig. 9. Effect of temperature on chalcocite dissolution. ( $[\text{Fe}^{3+}] = 10 \text{ g/dm}^3$ ,  $\text{pH} = 1.00\text{--}1.50$ ,  $E_h = 750 \text{ mV}$ , size fraction =  $-0.5+1 \text{ mm}$ )

### 3.4. Mineralogy

The 95% leached residue was examined to study the changes of mineral phases using X-ray Diffractometer and the result is shown in Fig. 10. Comparing with the XRD pattern of unleached sample (Fig. 1), it was noted that the ore was mainly composed of chalcocite and pyrite. However, as for the leach residue, it was observed that most of the strong peaks were found to be elemental sulfur and peaks of covellite were less and weak. This implied that the residue was mainly composed of elemental sulfur and covellite because of the incomplete dissolution.

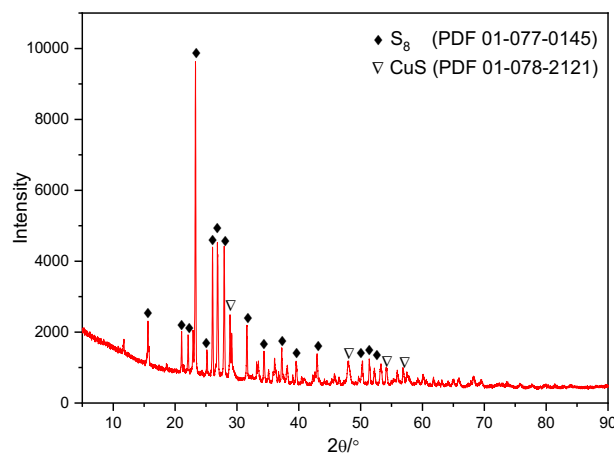


Fig. 10. X-ray pattern for residue of chalcocite mineral ( $-0.105+0.074 \text{ mm}$ )

SEM image and EDS analysis of chalcocite before leaching are illustrated in Fig. 11 and it can be seen that the chalcocite surface before leaching was rough and compact and EDS analysis also confirmed that copper and sulfur were major constituents on the surface. The BSE image of 60% leached chalcocite sample is presented in Fig. 12a and its related EDS analysis results are tabulated in Table 8. It could be noted that the number of cracks and pore networks were increased in the 60% leached chalcocite compared to chalcocite sample. From the XRD pattern of 60% leached chalcocite particles shown in Fig. 12b, it can be seen that peak for  $\text{Cu}_2\text{S}$  was rarely found while peaks of  $\text{CuS}$  phase and elemental sulfur was abundant. This result suggested that the transformation of  $\text{Cu}_2\text{S}$  to  $\text{CuS}$  was almost completed at 60% dissolution and this conclusion is also confirmed by the EDS results shown in Table 8. From Fig. 13, the surface of residue of different particle size were porous and harsh and the surface of residue of smaller particles (Fig. 13a) was seen to be composed of elemental sulfur. However, there was few

amounts of copper ion in the form of covellite on the larger residue surface (Fig. 13b-c). This finding agrees well with the dissolution for larger particle of incomplete dissolution. Another interesting finding in Fig. 13b-c is that small channels and cracks were formed on the surface. This finding was the evidence of the breakage of larger particles during dissolution which increased the surface area of particle. Consequently, the dissolution rate of larger particles became similar to that of smaller particles during the second stage of leaching and diffusion through sulfur product layer became rate-controlling factor.

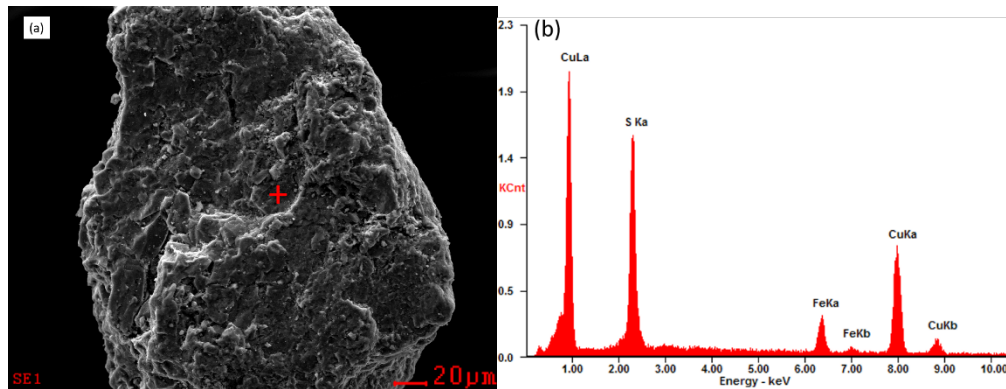


Fig. 11. SEM images of -0.5+0.105 mm of unleached chalcocite particles

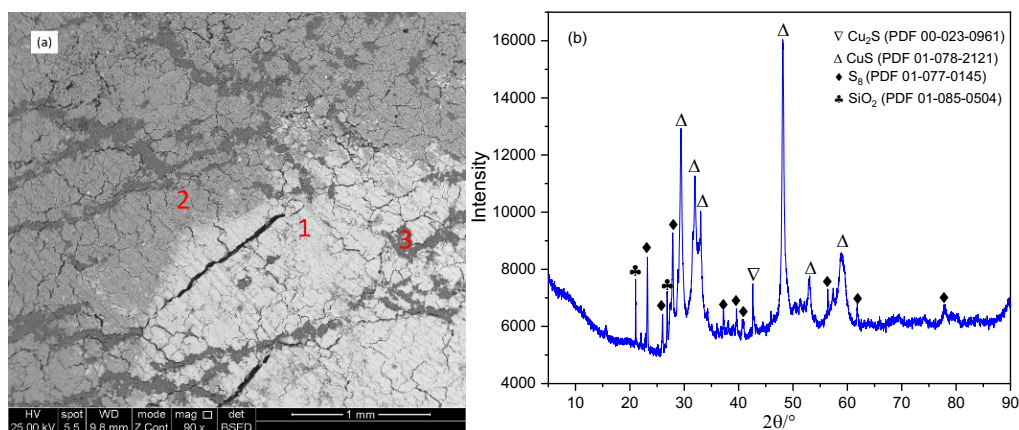


Fig. 12. a) BSE images and b) XRD pattern of 60% leached chalcocite

Table 8. EDS analysis of 60% leached chalcocite (at. %)

Number	Cu	S	Si	O
1	45.04	49.22	0.00	5.74
2	3.33	75.85	0.00	20.82
3	0.00	0.00	47.70	52.30

X-ray CT was used to investigate the changes in structures of sample before and after leaching because it can give 3-D mineral dissemination and crack distribution in large particles (Ghorbani et al., 2011). The acquired X-ray CT data was used to reconstruct using TXM 3D viewer for the image analysis. Fig. 14 shows the X-ray CT 2D images of chalcocite particles before and after leaching and Fig. 14a shows that the unleached particle was mainly composed of chalcocite and natural defects such as dents and pores to few extents. However, the number of pores and its network significantly increased and cracks were also formed on the leaching residue (Fig. 14b). It is concluded that the formation of crack was the proof of particle breakage during leaching. The reconstructed 3D images of chalcocite particles before and after leaching are shown in Fig. 15 and it was worth investigating that the compact structure of particle completely converted into porous and fractured particles after leaching.

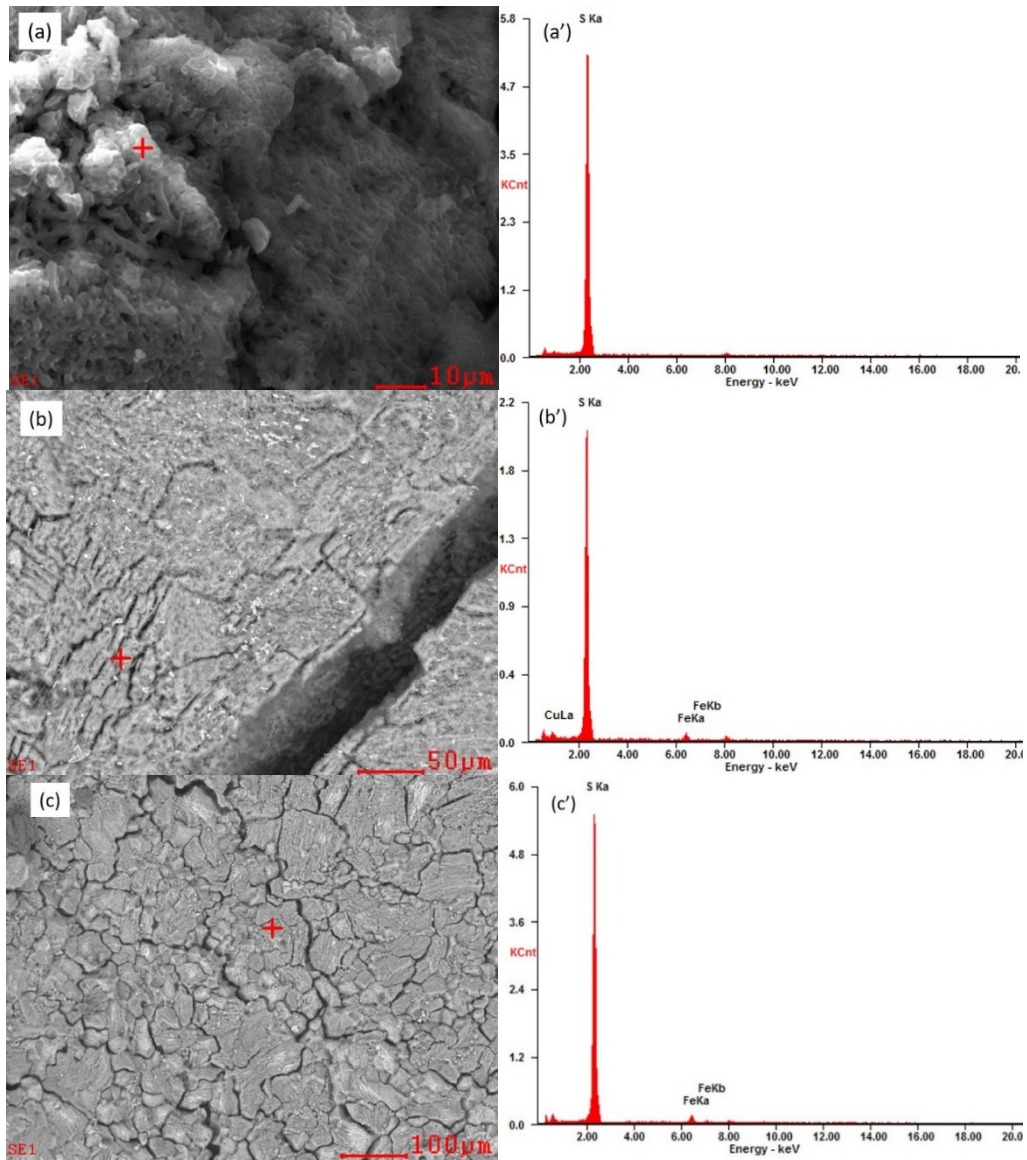


Fig. 13. SEM images of chalcocite residues of different particle sizes: (a)  $-0.074+0.054$  mm, (b)  $+1-0.5$  mm, (c)  $-4+2$  mm

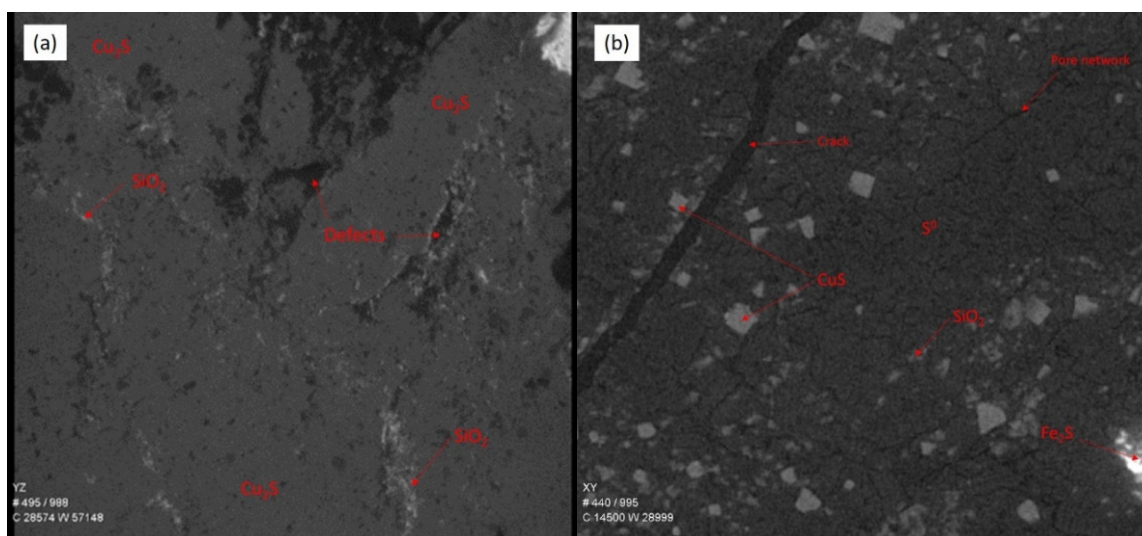


Fig. 14. X-ray CT images of chalcocite (a) before leaching and (b) after 95% leaching

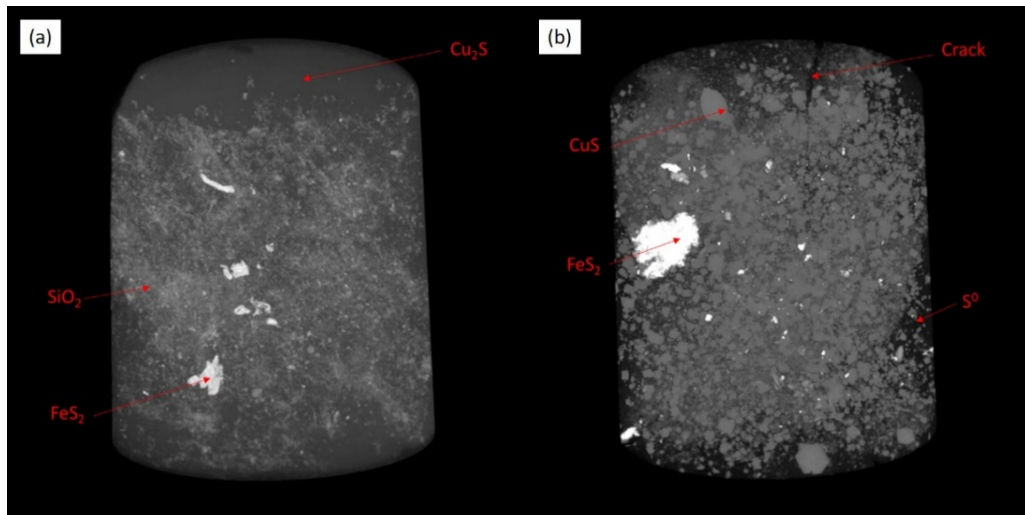


Fig. 15. 3D model of chalcocite after reconstruction (a) before leaching (b) after leaching

### 3.5. Implications for the heap bioleaching

The results of this research provided appropriate information to optimize heap bioleaching in practice.

1. The results of dissolution for particle sizes ranging from 0.054 to 200 mm suggested that particle size smaller than 31 mm should be used in order to optimize the performance of the heap because the dissolution of large particles was slow with low final dissolution compared with smaller particles.
2. The strong dependence of first stage dissolution kinetics on the particle size indicated that the particle size is one of the important parameters to control the dissolution rate before achieving the second stage. Dissolution of larger particles (31-200 mm) was more influenced by particle size rather than dissolution of smaller particles (0.054-31 mm). However, the slight effect of particle size on dissolution kinetics in second stage implied that particle size is not related to the slow leaching kinetics of second stage.
3. The investigation of particle breakage which leads to increasing surface area provided useful information for the shift of rate-determining steps from chemical reaction to product layer diffusion during second stage dissolution. The increasing number of pores at the end of dissolution process also suggested that diffusion of reactant and product accelerate dissolution rate of small particles. Based on the findings by SEM and X-ray CT data, the dissolution mechanism of large particles is demonstrated in Fig. 16.
4. The occurrence of high activation energies during the second stage dissolution implied that the dissolution can be enhanced by increasing the heap temperature. Similarly, sulfur layer became more porous at elevated temperature and allow to diffuse easily through it.

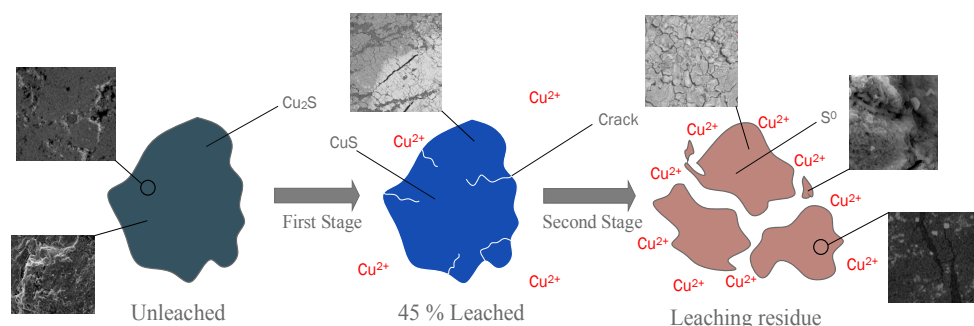


Fig. 16. Schematic diagram of leaching of chalcocite large particles

## 4. Conclusions

The dissolution of different particle sizes ranging from 0.054 to 200 mm of chalcocite ores in column leaching showed that particle size affected more obviously in the dissolution of large particle size (3.5-

200 mm) than that of small particle size (0.054-4 mm). Similarly, the particle size had significant effect on the first stage rather than second stages and the inflection point of the dissolution disappeared in the dissolution of larger particles (31-200 mm) whereas two inflection points were normally found in the dissolution of small particles (0.054-31 mm). Kinetics analysis of dissolution of small particle sizes (0.054-4 mm) revealed that the first stage was controlled by fluid diffusion while chemical reaction and product layer diffusion controlled the second stage. However, product layer diffusion control became significant with increasing particle size during the second stages of dissolution of small particle sizes. Similarly, the first stage dissolution of large particle sizes (31-200 mm) were controlled by product layer diffusion since the gangue mineral in low grade ore act as product layer. The product layer diffusion control also controlled the second stage due to the lack of inflection point in the leaching of large particle. Elevated leaching temperature was found to accelerate the rate of second stage leaching. X-ray CT and SEM-EDS studies confirmed that cracks and pores were considerably increased due to the particle breakage during the second stage. The mineralogical studies by SEM-EDS and XRD confirmed that the residue after dissolution of Cu from ore was mainly composed of elemental sulfur which was the major reason for slow kinetics in chalcocite leaching. For better understanding of the role of elemental sulfur layer on leaching kinetics, chalcocite is being bacterially leached using sulfur oxidizing bacteria, mainly, *Acidithiobacillus* to investigate the morphology of bacterially oxidized sulfur layer and its implications for kinetics.

### Acknowledgments

This research was supported by the National Natural Science Foundation of China (no.51674231); Key Research Program of Chinese Academy of Sciences (no. ZDRW-ZS-2018-1); Innovation Academy for Green Manufacture, Chinese Academy of Sciences (IAGM-2019A08). Authors gratefully acknowledged the support of State Key Laboratory of Biochemical Engineering and the help of Wanbao Mining Ltd.

### Nomenclature

- A: frequency factor
- b: stoichiometric coefficient
- $C_{fs}$ :  $Fe^{3+}$  concentration at the surface of the particle ( $mol/m^3$ )
- $D_e$ : effective diffusivity of sulfur layer ( $m^2/s$ )
- $E_a$ : activation energy (kJ/mol)
- k: rate constant
- $k_c$ : kinetic parameter for reaction control (1/s)
- $k_{cc}$ : chemical reaction rate constant (m/s)
- $k_f$ : kinetic parameter for film diffusion control (1/s)
- $k_l$ : mass transfer coefficient of the liquid film ( $m^3 \text{ liquid}/(m^2 \text{ surface} \cdot s)$ )
- $k_p$ : kinetic parameter for product diffusion control (1/s)
- M: molecular weight of particular sulfide mineral (kg/mol)
- $r_0$ : radius of original particle (m)
- R: universal gas constant (J/mol.K)
- $R^2$ : correlation coefficient
- t: time of reaction(s)
- T: temperature (K)
- x: fraction of reacted copper

### References

- ARACENA, A., CAMILA E., OSCAR J., DANILO C., ALDONZA J., 2019. *Dissolution kinetics of secondary covellite resulted from digenite dissolution in ferric/acid/chloride media*. Physicochem. Probl. Miner. Process. 55, 840-851.
- BOBECK, G., SU, H., 1985. *The kinetics of dissolution of sphalerite in ferric chloride solution*. Metall. Trans. B 16, 413-424.
- BOLORUNDURO, S.A., 1999. *Kinetics of leaching of chalcocite in acid ferric sulfate media: Chemical and bacterial leaching*. Phd thesis, The University of British Columbia.
- BRIERLEY, J.A., 2001. *Present and future commercial applications of biohydrometallurgy*. Hydrometallurgy 59, 233-239.

- CASTILLO, J., SEPÚLVEDA, R., ARAYA, G., GUZMÁN, TORO, N., PÉREZ, K., RODRÍGUEZ, M., NAVARRA, A., 2019. *Leaching of white metal in a NaCl-H<sub>2</sub>SO<sub>4</sub> system under environmental conditions*. Minerals 9, 319.
- CHENG, C.Y., FRANK, L., 1991a. *The kinetics of leaching chalcocite in acidic oxygenated sulphate-chloride solutions*. Hydrometallurgy 27, 249-268.
- CHENG, C.Y., FRANK, L., 1991b. *The kinetics of leaching covellite in acidic oxygenated sulphate-chloride solutions*. Hydrometallurgy 27, 269-284.
- CRUNDWELL, F.K., 2013. *The dissolution and leaching of minerals: Mechanisms, myths and misunderstandings*. Hydrometallurgy 139, 132-148.
- DEVECI, H., 2004. *Effect of particle size and shape of solids on the viability of acidophilic bacteria during mixing in stirred tank reactors*. Hydrometallurgy 71, 385-396.
- FANG, C., YU, S., WANG, X., ZHAO, H., QIN, W., QIU G., WANG, J., 2018. *Synchrotron radiation XRD investigation of the fine phase transformation during synthetic chalcocite acidic ferric sulfate leaching*. Minerals 8, 461.
- GEET, M.V., SWENNEN, R., WEVERS, M., 2000. *Quantitative analysis of reservoir rocks by microfocus X-ray computerised tomography*. Sediment. Geol. 132, 25-36.
- GHOORBANI, Y., BECKER, M., MAINZA, A., FRANZIDIS, J.P., PETERSEN, J., 2011. *Large particle effects in chemical/biochemical heap leach processes – a review*. Miner. Eng. 24, 1172-1184.
- GHOORBANI, Y., BECKER, M., PETERSEN, J., MORAR, S. H., MAINZA, A., FRANZIDIS, J.P., 2011. *Use of X-ray computed tomography to investigate crack distribution and mineral dissemination in sphalerite ore particles*. Miner. Eng. 24, 1249-1257.
- HASHEMZADEH, M., DIXON, D.G., LIU, W., 2019. *Modelling the kinetics of chalcocite leaching in acidified ferric chloride media under fully controlled pH and potential*. Hydrometallurgy 186, 275-283.
- JIA, Y., SUN, H.Y., TAN, Q.T., GAO, H.S., FENG, X.L., RUAN, R.M., 2018. *Linking leach chemistry and microbiology of low-grade copper ore bioleaching at different temperatures*. Int. J. Min. Met. Mater. 3, 271-279.
- LEVEBSPIEL, O.J., 1999. *Chemical reaction engineering*. John Wiley and Sons, N.Y, USA
- LIDDELL, K.C., 2005. *Shrinking core models in hydrometallurgy: What students are not being told about the pseudosteady approximation*. Hydrometallurgy 79, 62-68.
- MALMSTRÖM, M.E., BERGLUND, S., JARSJÖ, J., 2008. *Combined effects of spatially variable flow and mineralogy on the attenuation of acid mine drainage in groundwater*. Appl. Geochem. 23, 1419-1436.
- MAZUELOS, A., ROMOERO, R., RODRÍGUEZ, G, CARRANZA, F., 2001. *Ferric iron production in packed bed bioreactors: Influence of pH, temperature, particle size, bacterial support material and type of air distributor*. Miner. Eng. 4, 507-514.
- MIKI, H., NICOL, M., VELÁSQUEZ-YÉVENES, L., 2011. *The kinetics of dissolution of synthetic covellite, chalcocite and digenite in dilute chloride solutions at ambient temperatures*. Hydrometallurgy 105, 321-327.
- MILLER, G.M., 2003. *Ore geotechnical effects on copper heap leach kinetics*. Hydrometallurgy: Inter. Sympo. TMS.
- NADERI, H., ABDOLLAHY, M., MOSTOUFI, N., 2015. *Kinetics of chemical leaching of chalcocite from low-grade copper ore: Size-distribution behavior*. J. Min. Env. 6, 109-118.
- NAZEMI, M., RASHCHI, F., MOSTOUFI, N., 2011. *A new approach for identifying the rate controlling step applied to the leaching of nickel from spent catalyst*. Int. J. Miner. Process. 100, 21-26.
- NIU, X.P., RUAN, R.M., TAN, Q.Y., JIA, Y., SUN, H.Y., 2015. *Study on the second stage of chalcocite leaching in column with redox potential control and its implications*. Hydrometallurgy 155, 141-152.
- OGBONNA, N., PETERSEN, J., LAURIE, H., 2006. *An agglomerate scale model for the heap bioleaching of chalcocite*. J. S. Afr. I. Min. Metall. 106, 433-442.
- PÉREZ, K., JELDRES, R.I., NIETO, S., SALINAS-RODRÍGUEZ, E., ROBLES, P., QUEZADA, V., HERNÁNDEZ, J., TORO, N., 2020. *Leaching of pure chalcocite in a chloride media using waste water at high temperature*. Metals 10, 1-9.
- PÉREZ, K., TORO, N., SALDAÑA, M., SALINAS-RODRÍGUEZ, E., ROBLES, P., TORRES D., JELDRES, R.I., 2020. *Statistical study for leaching of covellite in a chloride media*. Metals 10, 477.
- PETERSEN, J., DIXON, D.G., 2007. *Principles, mechanisms and dynamics of chalcocite heap bioleaching*, In Microbial processing of metal sulfides. Springer. 193-218.
- RUIZ, M.C., HONORES, S., PADILLA, R., 1998. *Leaching kinetics of digenite concentrate in oxygenated chloride media at ambient pressure*. Metall. Mater. Trans. A 29, 961-969.
- SCHIPPERS, A., SAND, W., 1999. *Bacterial leaching of metal sulfides proceeds by two indirect mechanisms via thiosulfate or via polysulfides and sulfur*. Appl. and Environ. Microbiol. 65, 319.

- STRÖMBERG, B., BANWART, S.A., 1999. *Experimental study of acidity-consuming processes in mining waste rock: Some influences of mineralogy and particle size*. Appl. Geochem. 14, 1-16.
- SUNI, J., HENEIN, H., WARREN, G.W., Reddy, D., 1989. *Modelling the leaching kinetics of a sphalerite concentrate size distribution in ferric chloride solution*. Hydrometallurgy 22, 25-38.
- TORO, N., BRICEÑO, W., PÉREZ, K., CÁNOVAS, M., TRIGUEROS, E., SEPÚLVEDA, R., HERNÁNDEZ, P., 2019. *Leaching of pure chalcocite in a chloride media using sea water and waste water*. Metals 9, 780.
- VIDELA, A.R., LIN, C.L., Miller, J.D., 2007. *3d characterization of individual multiphase particles in packedparticle beds by X-ray microtomography (XMT)*. Int. J. Miner. Process. 84, 321-326.
- WATLING, H.R., 2006. *The bioleaching of sulphide minerals with emphasis on copper sulphides – a review*. Hydrometallurgy 84, 81-108.